# Thermo-elastic wavefront and polarization error analysis of a telecommunication optical circulator

Keith B. Doyle
Optical Research Associates
Westborough, MA

William M. Bell
Topsfield Engineering Service, Inc.
Hingham, MA 02043

## ABSTRACT

Loss in optical fiber coupling efficiency and transmission are computed for a telecommunication optical circulator. Optical performance degradation is due to thermally induced optical errors in the two beam splitter cubes. The computation of the optical errors is discussed for two materials and the effects illustrated. Bulk volumetric absorption of the incident laser radiation from the input optical fiber and surface absorption via the coatings on the beam splitter interface generate temperature gradients. Loss in optical fiber coupling efficiency is produced by wavefront error caused by thermal expansion effects, and refractive index changes with temperature and stress. Transmission loss in the optical circulator is caused by polarization errors generated by the effects of stress birefringence. The optical errors were computed using temperatures generated from a Thermal Desktop model and displacements and stresses generated by a MSC/Nastran finite element model. The optical errors were imposed upon a Code V optical model to compute loss in fiber coupling efficiency and transmission in the optical circulator.

**Keywords**: Beam splitter cubes, wavefront error, fiber coupling efficiency, optical circulator, stress birefringence, thermo-elastic analysis

## 1. INTRODUCTION

Numerous passive components are being developed for use in conjunction with optical fiber and telecommunication technology to modify and process optical signals. The degree to which the optics depart from the design due to misalignments, fabrication, and induced environmental errors cause loss in optical fiber coupling efficiency. Furthermore, polarization changes affect transmission characteristics of the optical system. A number of these passive components in the telecommunications industry use polarization beam splitter cubes including optical circulators. A critical source of optical error may be induced by temperature changes due to the environment and/or the incident radiation. A portion of the radiation traversing the optical element is absorbed volumetrically in the base optical material, the coating materials on the beam splitter interface, the residual polishing compounds, and by inhomogeneities in the optical material within the radiation path. The temperature gradients within and on the surface of the optical elements will vary depending on the location and quantity of energy absorbed and the ability of the optical elements to dissipate this energy to the surrounding environment. These temperature gradients will be non-linear and produce several deleterious effects. The first effect is the thermal expansion/contraction of the optical material which produces wavefront error. The second effect is the change in the index of refraction of the optical material as a function of temperature which also produces wavefront error. A third effect is generated by the resulting state of stress. This state of stress, for stress-sensitive materials, changes the materials' index of refraction as a function of direction i.e. produces anisotropic optical behavior. This effect will cause both wavefront error and polarization changes. The prediction and assessment of these optical errors can be important for high data rate systems. In particular, beamsplitter cubes present special challenges in these optical systems due to their size. The optical path within the beamsplitter is typically much greater than that of other optical elements within the system and hence the aforementioned optical errors are more severe and tend to degrade system performance. This paper discusses the analytical methods to predict thermally induced optical errors and addresses the thermal-structural-optical modeling to predict overall optical performance for the case of an optical circulator.

## 2. THERMAL INDUCED OPTICAL ERRORS

The computation of thermally induced optical errors developed in the beam splitter cubes is discussed. The effect of the temperature changes on the optical path difference due to thermal expansion and index of refraction changes due to temperature is given by:

$$\delta_T = \left( \alpha(n-1) + \frac{\partial n}{\partial t} \right) L \Delta T \tag{1}$$

where:

$\delta_T$ is the peak wavefront error due to temperature, $\alpha$ is the coefficient of thermal expansion, n is the index of refraction, $\Delta T$ is the temperature change, L is the length of the ray within the optical element, and the temperature coefficient of refractive index is denoted by $\frac{\partial n}{\partial t}$.

For many transparent optical materials, the application of mechanical stress causes optical anisotropy i.e. the refractive index of the material is a function of direction. This is known as the photoelastic effect[1] and causes wavefront error and alters the polarization state of the incident wave. This effect is governed by the following fourth rank tensor transformation:

$$\Delta\beta_{ij} = q_{ijkl}\sigma_{kl} \tag{2}$$

where B is the dielectric impermeability and q represents the stress-optical coefficients. For an isotropic material exhibiting stress birefringence there are two stress optical coefficients. The stress-optical coefficient matrix is as follows:

$$q = \begin{bmatrix} q_{11} & q_{12} & q_{12} & 0 & 0 & 0 \\ q_{12} & q_{11} & q_{12} & 0 & 0 & 0 \\ q_{12} & q_{12} & q_{11} & 0 & 0 & 0 \\ 0 & 0 & 0 & q_{44} & 0 & 0 \\ 0 & 0 & 0 & 0 & q_{44} & 0 \\ 0 & 0 & 0 & 0 & 0 & q_{44} \end{bmatrix} \quad where \;\; q_{44} = \frac{q_{11} - q_{12}}{2} \tag{3}$$

To compute the effects of stress birefringence for a given ray path, the principal stresses in the plane perpendicular to the ray direction must be determined. Thus a stress transformation must be performed to orient one of the planes of the stress tensor to be perpendicular to the ray direction. (In this case, a stress transformation is performed to orient the z-axis to be parallel with the ray direction.) Next, the principal stresses and the rotation angle in the xy-plane, $\theta_{xy}$ are determined for the plane normal to the ray direction. This determines the direction of the principal indices of refraction, which are coincident with the principal stress directions. At each point of the stressed body which the ray traverses, the input polarized light is then resolved into two mutually perpendicular components lying in the planes of the principal stresses. This yields the following dielectric impermeability tensor:

$$\Delta\beta_{ij} = \begin{bmatrix} q_{11}\sigma_{11} + q_{12}(\sigma_{22}+\sigma_{zz}) \\ q_{11}\sigma_{22} + q_{12}(\sigma_{11}+\sigma_{zz}) \\ q_{11}\sigma_{33} + q_{12}(\sigma_{11}+\sigma_{22}) \\ 0 \\ q_{44}\sigma_{yz} \\ q_{44}\sigma_{xz} \end{bmatrix} \tag{4}$$

where $\sigma_{11}$ and $\sigma_{22}$ are the principal stresses in the xy-plane and $\sigma_{zz}$, $\sigma_{xz}$, and $\sigma_{yz}$ are the stress terms based on the z-axis oriented parallel with the direction of the ray. The changes in refractive index in the two principal directions for small changes in optical properties are given by[2]:

$$\Delta n_1 = -\frac{1}{2} n^3{}_o \Delta\beta_{11} = -\frac{1}{2} n^3{}_o [(q_{11}\sigma_{11} + q_{12}(\sigma_{22} + \sigma_{zz})] \quad (5)$$

$$\Delta n_2 = -\frac{1}{2} n^3{}_o \Delta\beta_{22} = -\frac{1}{2} n^3{}_o [(q_{11}\sigma_{22} + q_{12}(\sigma_{11} + \sigma_{zz})] \quad (6)$$

The phase retardations due to the index changes in the principal directions produces wavefront error and as given by:

$$\delta_1 = \frac{2\pi\Delta n_1 L}{\lambda} \quad (7)$$

$$\delta_2 = \frac{2\pi\Delta n_2 L}{\lambda} \quad (8)$$

The effects of stress birefringence on the wavefront error and output polarization state for each traced ray path were computed based on a technique outlined by Yiu and Meyer[2]. The use of Jones Calculus allows computation of retarder and rotation matrices based upon the resultant stress field in each finite element that the ray traverses. Successive matrix multiplications of these matrices generates the resultant wavefront error for each orthogonal component of polarization and the output polarization state. The retarder and rotation matrices, respectively, are shown below.

$$R(\delta) = \begin{bmatrix} e^{i\delta_1} & 0 \\ 0 & e^{i\delta_2} \end{bmatrix} \quad (9)$$

$$R(\theta) = \begin{bmatrix} \cos\theta & \sin\theta \\ -\sin\theta & \cos\theta \end{bmatrix} \quad (10)$$

For each element, the following matrix multiplication is performed:

$$E_i = R(\theta)_i^T R(\delta)_i R(\theta)_i \quad (11)$$

A system level matrix is generated by multiplying together each element matrix, $E_i$. The system level matrix is then multiplied by the input polarization state to yield the output polarization state. For unpolarized light, the initial rotation matrix angles are set to zero, and the amplitudes for the input state are set equal. The effects of ray splitting due to birefringence is ignored in the analysis, as is the effects of angular ray deviations produced by any surface and wavefront deformations e.g. the input rays are assumed to travel in straight lines through the beam splitter cube.

## 3. OPTICAL CIRCULATOR / OPTICAL MODEL ANALYSIS

In the telecommunication field, optical circulators are used for several applications including bi-directional transmission, WDM networks, and fiber amplifier systems. The function of a circulator is to redirect light from port-to-port, sequentially, in one direction only. In this example, light entering the circulator at port one, leaves the circulator at port two. A schematic of the optical circulator is shown in Figure 1 (U.S. Pat. No. 5,204,771 by Kuwahara). An unpolarized gaussian beam leaves the input optical fiber and is collimated prior to entering the optical circulator at port 1. The light enters the polarization beam splitter (PBS) #1 and half the energy is transmitted straight through the cube as p-polarization and half the energy is reflected 90-degrees as s-polarization. The two beams next traverse a 45-degree Faraday rotator and a polarization compensator, which convert the s-polarization state to p-polarization and vice versa. The two beams then enter PBS #2 where the two beams are recombined (p-polarization passes straight through the beam splitter and s-polarization is reflected) and exit the cube at port 2. The beams are then coupled into the output optical fiber. It is assumed that no other optical errors exist within the system other than thermally induced optical errors of the beam splitter cube.

The first effect of the optical errors considered is the loss of the light leaving port 1 and entering port 2 (light leaving port 1 and entering port 4 i.e. cross talk). Once the s-state and p-state polarized light are separated at the first beam splitter cube interface, the polarization states will be altered via stress birefringence as the beams traverse the second half of the PBS #1 and the first half of PBS #2 (the ray path within the PBS cube prior to hitting the beam splitter interface). The effects of stress birefringence convert the linear polarized light into elliptical states of polarization. The orthogonal components that are generated, resulting in the elliptical state, are transmitted to port 4. The percentage of this light lost is computed as the loss in transmission. A 30-dB loss to port 4 is considered significant.

The second effect of the optical errors is to reduce the optical fiber coupling efficiency. Surface and wavefront errors are added to the Code V model of the optical circulator to compute the fiber coupling efficiency loss. Interferogram (INT) files are used to model the optical perturbations. The wavefront INT file is used to account for index of refraction changes due to temperature and stress. This form of the INT file modifies the ray deviations and OPD but does not effect the surface. The surface INT file is used to represent optical surface deformations of the beam splitter cube. During ray tracing, the additional deformation, including the refractive index and angle of incidence are taken into account when calculating ray deviations or OPD. A third type of interferogram file allows the user to specify birefringence data. This feature accounts for the magnitude of stress birefringence, specified as the difference in optical path difference between the e-ray and the o-ray, and the orientation of the crystal axis. A flow-chart depicting the inter-disciplinary modeling is shown in Figure 2.

The optical errors were computed for two potential materials for the beam splitter cubes - fused silica and BK7. The material properties are given in Table 1. The temperatures in the beam splitter cube were computed using the thermal properties of fused silica. This temperature distribution was also used to compute the optical errors for BK7. This neglected the differences in bulk absorption and conductivity of BK7 as compared to fused silica. The dominant properties governing the optical errors are the thermal coefficient of refractive index, and the coefficient of thermal expansion values, which vary by more than a factor of ten between the two materials. Hence the temperature difference between the two materials was considered insignificant in the overall analysis.

## 4. THERMAL ANALYSIS

The temperature changes induced in the beamsplitter cube due to the radiation from the input optical fiber were computed using the thermal analysis software program Thermal Desktop. Present thermal analysis software is not capable of bulk volumetric energy absorption in solid, transmissive elements. This software, however, is capable of energy absorption on plate elements of “zero” thickness. Hence, a two-stage analysis was required to compute the temperature change. The first step was to develop a heat rate model to determine the energy absorbed by the beamsplitter cube material using plate elements. The second step involved transferring the nodal heat rates, determined in the plate elements, to a thermal network model. Then, using SINDA/FLUINT, the steady-state temperature distribution of the cube was calculated as the absorbed energy was conducted out to the cube surfaces and then conducted, convected, and radiated to the surrounding environment.

A gaussian beam exits the input optical fiber and enters the beam splitter cube with a total power of 100 milliwatts at a wavelength of 1550 nm**.** The gaussian beam waist diameter is 6 mm. The percent of energy absorbed by the beam splitter cube material was estimated using data from Corning on the material fused silica. The absorption coefficient of the beam splitter interface was provided via data from the customer (2% of the incident radiation was assumed absorbed by the coating).

Using Thermal Desktop, there are a number of ways to emulate the energy beam characteristics. These include the following:

- Use of a heated source whose surface radiates a specific amount of energy in the correct shape, direction, and intensity.
- Use of multiple heat sources surfaces with varying intensity.
- Use of optical elements, such as lenses, to focus and direct the energy beam.
- Use of masks to contour the beam.
- Use of varying absorption coefficients in the beam path to emulate non-uniform intensity distributions
- Use of absorption coefficients that vary with angle of incidence.

For this effort, a simple collimated beam heat source of 100 milliwatts was used to demonstrate the overall analysis techniques.

The energy absorbed by bulk volumetric absorption was computed using plate elements of zero thickness. These plate elements represent a volumetric portion of the beamsplitter cube. They are assigned an effective absorptivity that will cause the element to absorb the amount of energy that would be absorbed by the solid that it represents, and transmit the remainder. These plate elements are also assigned a transmissive specularity of 1.0. The model was setup as a two-dimensional series of parallel plate elements (normal and perpendicular to the direction of the incident radiation) to account for energy flow in two-directions, and a diagonal plane representative of the beam splitter interface. Each plate element was subdivided into 225 nodes (15 x 15). The beamsplitter interface plate element was assigned an effective absorptivity that caused the element to absorb the amount of energy that would be absorbed by the coated surface, reflecting and transmitting the remainder with a transmissive specularity of 1.0.

The Thermal Desktop run of the radiation model, using Monte Carlo techniques and a sufficient number of rays, generated a tabulation of energy absorption for each node in the multiple plate model. Care was taken to assure that the total energy flow was accounted for, and the energy distribution was accurate.

A thermal network model of the beamsplitter cube, subdivided into 3,375 nodes (15x15x15), was created using Sinda/Fluint to predict steady-state temperatures, given the beam energy absorption and the surrounding environmental conditions. For simplicity, the beamsplitter was modeled as sitting in space with six sides radiating and convecting to the environment. The surrounding environment was considered a black cavity at 22 C. The thermal emissivity of the surfaces of the cube was set at 0.9. Convection was assumed to be “natural” and was computed for the six-sides based on the temperature difference from the cube surface to the environmental air temperature. Heat rates from the preceding analysis are applied to the nearest node in the thermal network model. All of the thermal network nodes are conductively connected to adjacent nodes or the environment with radiation and convection conductors. The beam splitter cube is assumed to be in a conducting isolated perfect kinematic mount in the analysis, and any thermal and structural effects induced by a non-ideal mount are ignored. Also note that the environment itself could in some cases be significantly non-uniform, and thus create larger temperature gradients within the beamsplitter cube.

The temperature distribution in the beam splitter cube ranged from 23.1 C to 26.2 C. The highest temperatures are at the center of the cube which absorb the largest amount of the radiation due to the absorption at the coating on the beamsplitter interface. Asymmetries exist in the beamsplitter cube temperature distribution due to the differences in the convective flow between the top and bottom faces, and the path of the incident and reflected radiation. A slight non-symmetrical temperature distribution is observed between the top and bottom faces (with the warmer temperatures on the bottom), and a non-symmetrical left-to-right temperature distribution also exists (due to half of the incident radiation passing directly through the cube and the other half being reflected out the side of the cube). These nodal temperatures were mapped to the nodes of the structural model using Thermal Desktop. The beam splitter temperature distributions are shown on the finite element model in Figure 3. Further asymmetries could exist in the beam splitter cube temperature distribution due to the packaging configuration of the optical circulator, more differences in convection flow between the top and bottom faces, the path of the incident radiation, and a surrounding non-uniform radiation environment.

## 5. STRUCTURAL ANALYSIS

A MSC/Nastran finite element model of the beam splitter cube was created. An undeformed view of the finite element model, along with the global coordinate system, is shown in Figure 4. The optical axis is along the global z-axis and the incident light enters the minus Z face. Each side of the beam splitter cube is 8.7 mm. The model consisted of a 15 x 15 x 16 element mesh resulting in the generation of 4096 structural nodes. The model was constructed such that nodes existed along the geometric diagonal of the cube. Kinematic constraints were applied such that the induced model deformation and stress were a result of the applied temperature distribution.

A greatly exaggerated view of the finite element model deformation is shown in Figure 5. The highest temperatures exist in the center of the cube while the faces of the cube were at cooler temperatures. This resulted in compressive stresses in the center of the cube due to constrained thermal growth. The faces of the cube where radiation passes have higher temperatures at the center as compared to the edges. This generates a convex shape and thus tensile bending stresses on the lateral faces. The maximum principal stresses generated in the cube were 234 psi. The minimum principal stresses were -212 psi.

## 6. WAVEFRONT AND POLARIZATION ERROR ANALYSIS

The temperature and stress distributions within the beam splitter cubes were used to compute the optical errors. The beam splitter surface displacements, computed by the finite element model, of the entering, exiting, and interface planes were fit to

Zernike Polynomials and output into Code V surface INT files using a Matlab program. For analytical simplification, the amount of energy loss due to reflection, bulk volumetric absorption, and coating absorption was neglected in figuring inputs to PBS #2, so the temperature, displacement, and stress fields were identical (aside from a 180-degree rotation) for the two beam splitter cubes in the optical circulator. Thus, four surface INT files describe the displacements for the two beam splitter cubes.

Wavefront errors generated by the changes in index of refraction due to temperature changes were computed using a Matlab program. A square grid of twenty-five rays was passed through the beam splitter cube with index changes summed as the ray traversed each element of the thermal model. This computation was performed twice to account for rays that traveled through the beam splitter interface and exited out the rear face and for the rays that were reflected at the beam splitter interface (re-directed 90-degrees) and exited out the side of the cube. The index changes were then interpolated to a 51 x 51 grid, fit to Zernike polynomials, and output as Code V wavefront INT files.

Wavefront and polarization errors generated by the stresses in the beam splitter were computed by tracing twenty-five rays through the finite element generated stress field. A Matlab program computed the rotation and retarder matrices for each finite element that the ray traversed and successive multiplication of these matrices allowed the determination of the wavefront error for each orthogonal component and the output polarization state. This calculation was performed twice to account for rays passing straight through the cube and exiting out the rear face and for the rays reflecting off the beam splitter interface and exiting out the side face. The stress-induced retardance for each orthogonal component (s and p-polarization states) for the 25 rays was interpolated to a 51 x 51 grid, fit to Zernike polynomials, and output to wavefront INT files. The effects of stress birefringence were accounted for by using birefringent INT files. The first beam splitter interface converts the unpolarized light into the two orthogonal s and p-polarization states. The polarized states pass through the stress fields of the second half of the first beam splitter and the first half of the second beam splitter (path prior to the beam splitter interface) which cause each linear polarized state to become elliptical due to the stress birefringence The retardance difference values for the 25-rays were used to generate birefringent magnitude INT files and the ratio of the amplitudes were used to create the orientation INT files. The birefringent INT files were placed on a dummy surface at the second beam splitter interface.

## 7. RESULTS

Loss in optical fiber coupling efficiency and transmission was computed and compared using two beam splitter cube materials – fused silica and BK7. The results were based on the assumption that the temperature distribution in the cube was the same for both materials. The loss in fiber coupling efficiency is governed by the surface error of the faces of the cube, and the wavefront error due to the temperature and stress fields. The rms surface error of the faces of the beam splitter cube for the two materials are shown in Table 2. As expected the displacements for the fused silica cube are over an order of magnitude less than the displacements for the BK7 cube due the CTE difference between the materials. Contour maps of the surface error for the four relevant surfaces are shown in Figures 6-9. The errors for the three exterior surfaces are dominated by piston and focus error. The dominant error for the beam splitter interface is tilt.

The wavefront error due to the temperature and stress-induced changes in the index of refraction for the two materials are shown in Table 3. The stress-induced wavefront error in fused silica is more than an order of magnitude less than that of BK7. This is explained, again, by the CTE difference between the two materials. Contour maps of the stress-induced wavefront error for the optical circulator (i.e. the combined effects of the two beam splitter cubes) are shown in Figure 10. The primary errors are focus and spherical aberration. On the other hand, the wavefront error due to the temperature induced changes in refractive index for fused silica are an order of magnitude greater than that of BK7. This is due to the difference in the thermal coefficient of refractive index. Contour maps for the wavefront error (combined effects of the two beam splitter cubes) due to index of refraction changes with temperature are shown in Figure 11. The dominant error is again focus and spherical aberration.

The optical coupling efficiency for the optical circulator, for both materials, was computed using Code V (see Table 4). The optical coupling loss, expressed in dB, for fused silica was –0.46 dB**.** The optical coupling loss, using BK7 as the beam splitter cube material, was –0.11 dB. Optical coupling loss on the order of 0.25 to 0.5 dB begin to present problems for high data rate telecommunication systems. Optical errors in other system components and misalignments will further degrade coupling efficiency.

The loss in transmission of the optical circulator was also computed using Code V. The transmission loss from light leaving port 1 to port 2 (i.e light lost to port 4), as caused by stress birefringence, was considered negligible. This result may be

explained by the fact that the majority of the energy in the gaussian beam traverses a stress field that is void of shear stresses in the plane normal to the ray direction. Thus, the x and y-axes of the ray coordinate system define the principal axes and the rotation angle is zero. For an initial linearly polarized ray, the resulting stress state retards each component of the polarization vector but it does not affect the amplitude, and thus the transmission characteristics remain relatively unchanged. For a change in amplitude to occur in the s- and p-polarization states, there must exist a rotation angle in the plane normal to the ray between the ray coordinate system and the principal coordinate system. The stress fields near the edges of the cube, and in particular the corners, exhibit significant shear stresses. However, the energy in the gaussian beam at the edge of the cube is insignificant resulting in little overall transmission loss.

## 8. CONCLUSION

Optical fiber coupling and transmission losses were computed for a telecommunication optical circulator based on optical errors in the beam splitter cubes. The analysis was performed for two potential material choices for the beam splitter cubes – fused silica and BK7. A Code V optical model was used to compute the fiber coupling efficiency and transmission loss based on errors applied to the model through interferogram files. Thermal and structural models were used to generate the temperature, displacement, and stress distributions in the beam splitter cubes. Matlab programs were used to transform the data into the appropriate interferogram file format to perturb the optical model. For fused silica, the optical errors were dominated by refractive index changes due to temperature. Conversely, for BK7 the optical errors were a result of structural effects. Surface distortions of the beam splitter surfaces and stress-induced index of refractive changes for BK7 dominated index of refraction changes due to temperature. These results are explained by the order of magnitude difference in the coefficient of thermal expansion and the temperature coefficient of refractive index between the two materials. The effect of the optical errors on optical coupling efficiency for BK7 is to produce a coupling loss of –0.11 dB. The optical errors in fused silica generated a coupling loss of –0.46 dB. The transmission loss due to stress birefringence was determined to be negligible. This may be explained by the lack of shear stresses in the beam splitter cubes. Thus the principal stress axes are coincident with the ray coordinate axes, and the linearly polarized wave stays nearly linear after passing through the stress fields.

## REFERENCES


[1]American Institute of Physics Handbook, 2nd Edition, Dwight E. Gray, Editor, McGraw-Hill Book Company, 1963.

[2]Yiu, Y. C. and Meyer, A. R., Computation of Optical Errors in Transparent Optical Elements due to Three Dimensional Photoelastic Effect, Proceedings of SPIE – the International Society for Optical Engineering, Vol. 1303, 1990.


## TABLES

| MATERIAL PROPERTIES | BK7 | FUSED SILICA |
|---|---|---|
| Elastic Modulus (mpsi) | 11.7 | 10.6 |
| Poisson Ratio | 0.206 | 0.176 |
| CTE (ppm/C) | 7.1 | 0.56 |
| Thermal-Optic (x $10^6$) | 0.9 | 11.1 |
| Stress-Optic,$q_{11}/q_{12}$ ($in^2/lb$ x$10^8$) | -0.35/-2.9 | -2.2/-4.4 |

Table 1. Material Properties

| RMS SURFACE ERROR (λ AT 1550 NM) | | |
|---|---|---|
| X1000 | BK7 | Fused Silica |
| Front | 9.6 | 0.75 |
| Rear | 9.7 | 0.76 |
| Side | 11.0 | 0.83 |
| Interface | 12.0 | 0.92 |

Table 2. Beam Splitter Surface Errors

| WAVEFRONT ERROR RMS (λ AT 1550 NM) | | |
|---|---|---|
| X1000 | BK7 | Fused Silica |
| Temperature | 7.0 | 84.0 |
| Stress | 19.5 | 1.0 |

Table 3. Temperature and Stress-Induced WFE

| OPTICAL COUPLING LOSS (DB) | |
|---|---|
| BK7 | Fused Silica |
| -0.11 | -0.46 |

Table 4. Optical Coupling Loss

# FIGURES

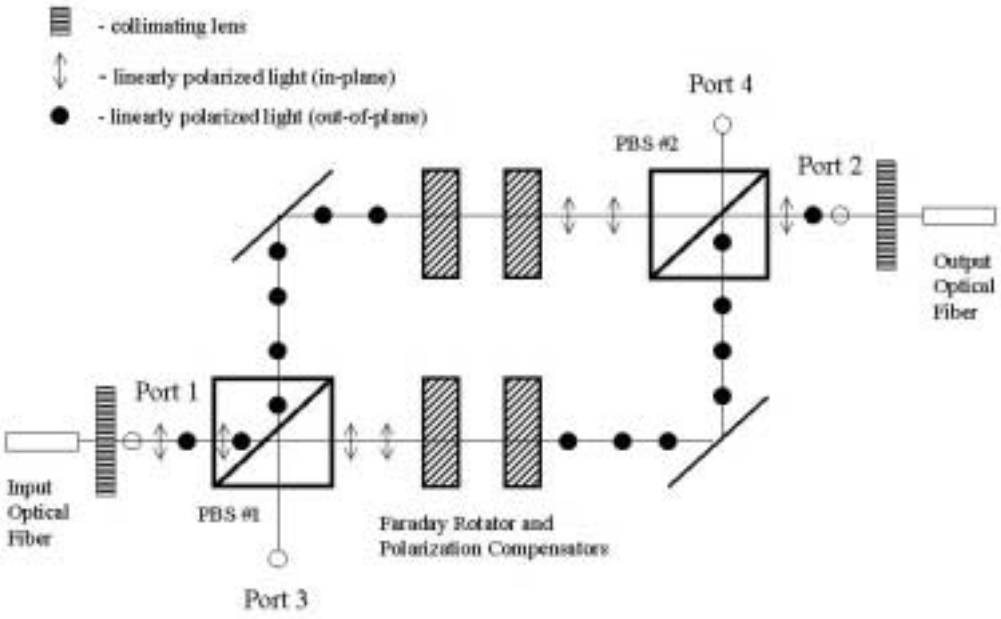


Figure 1. Optical Circulator Schematic

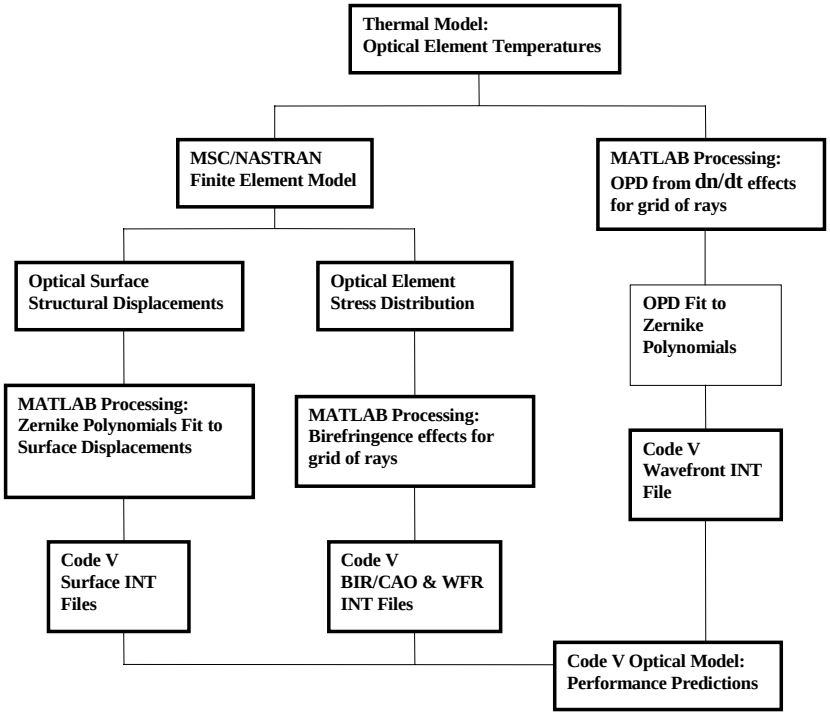


Figure 2. Integrated Modeling Flow-Chart

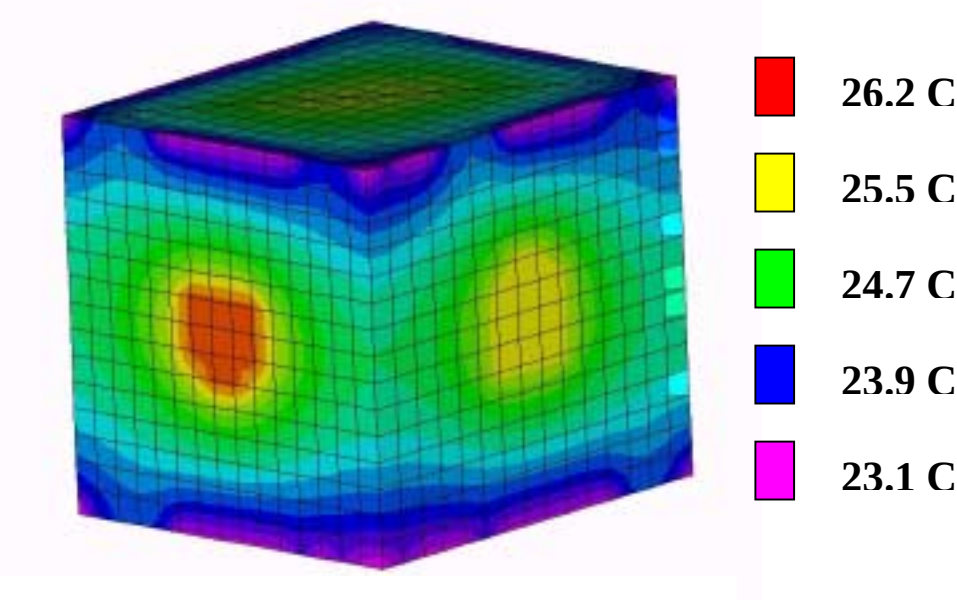


Figure 3. Beam Splitter Cube Temperature Contour Map

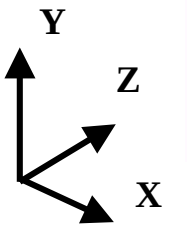


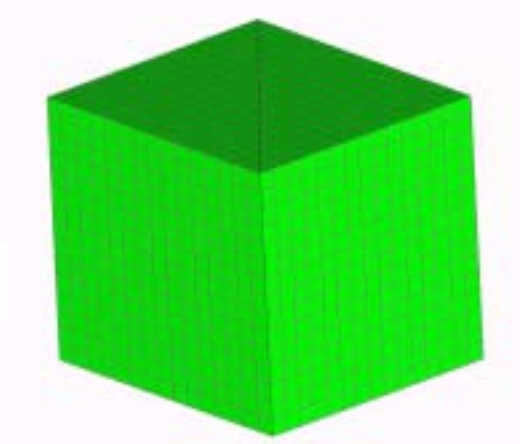

Figure 4. Beam Splitter Cube
Finite Element Model

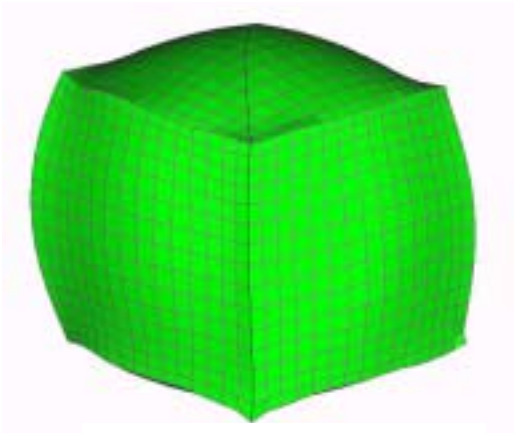

Figure 5. Beam Splitter Cube
Deformed Shape

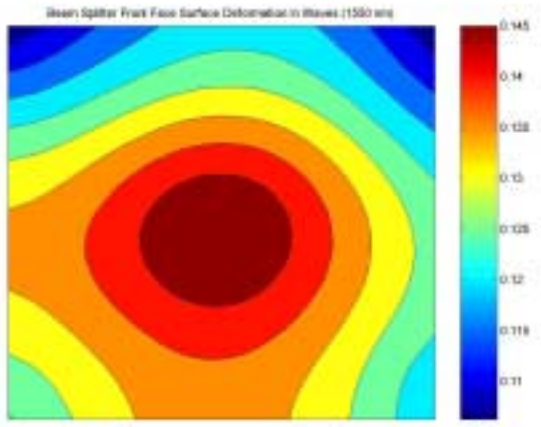

Figure 6. Cube Front Surface Error Contour Map (BK7)

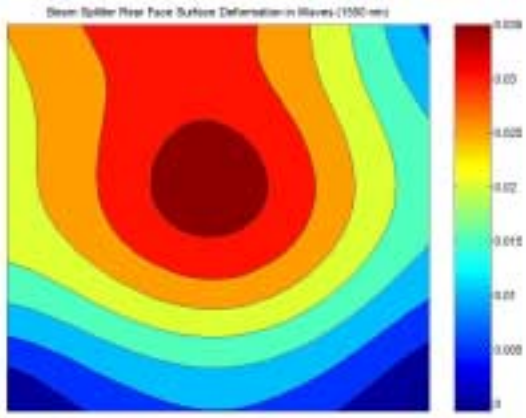

Figure 7. Cube Rear Surface Error Contour Map (BK7)

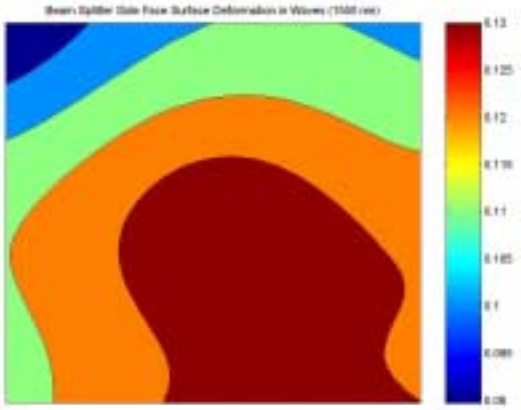

Figure 8. Cube Side Surface Error Contour Map (BK7)

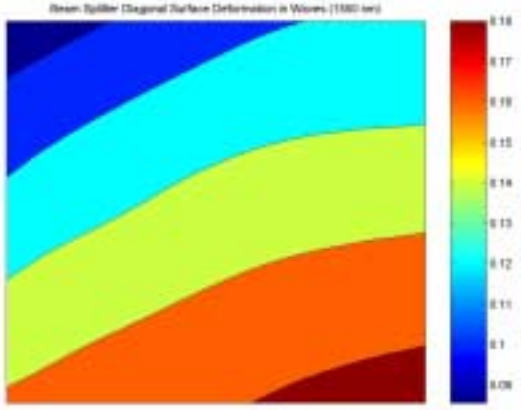

Figure 9. Cube Diagonal Surface Error Contour Map (BK7)

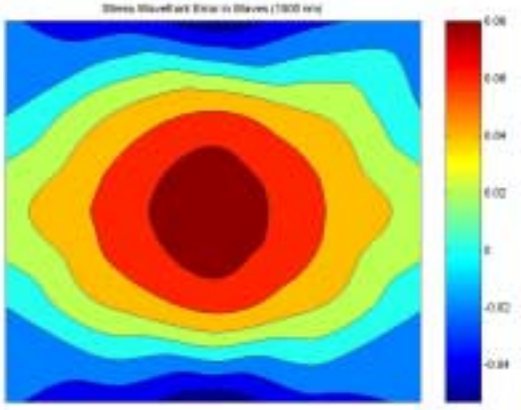

Figure 10. Stress-Induced Wavefront Error Contour Map (BK7)

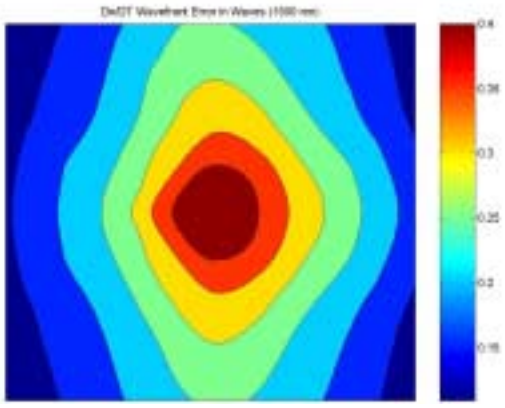

Figure 11. Temperature-Induced Wavefront Error Contour Map (Fused Silica)